Nano Energy 73 (2020) 104772

Contents lists available at ScienceDirect

Nano Energy

journal homepage: http://www.elsevier.com/locate/nanoen

A soft robotic finger with self-powered triboelectric curvature sensor based on multi-material 3D printing

Mingzhu Zhu [a,c], Mengying Xie [b,c,*], Xuanming Lu [d], Shima Okada [e], Sadao Kawamura [e]

[a] Information Engineering College, Zhejiang University of Technology, Hangzhou, 310023, China
[b] State Key Laboratory of Precision Measuring Technology and Instruments, School of Precision Instrument and Optoelectronics Engineering, Tianjin University, Tianjin, 300072, China
[c] Ritsumeikan Global Innovation Research Organization, Ritsumeikan University, Kusatsu City, 525-8577, Japan
[d] Research Department of Intelligent Manufacturing Equipment, Nanjing Institute of Technology, Nanjing, 211167, China
[e] Department of Robotics, Ritsumeikan University, Kusatsu City, 525-8577, Japan

ARTICLE INFO

Keywords:
Triboelectric
Self-powered curvature sensor
Soft robotics
Multi-material 3D printing
Single electrode

ABSTRACT

Significant advances in the area of additive manufacturing have provided a novel fabrication method to develop soft robots with self-powered sensors. In this paper, multi-material 3D printing is used to directly print a soft robotic finger with a triboelectric curvature sensor. The reinforced soft finger with a single-electrode triboelectric curvature sensor (RSF-S-TECS) combines the advantages of multi-material 3D printing and stretchable electrodes to achieve fast prototyping and easy system integration. The triboelectric curvature sensor is located on the top of the finger, where one active layer of the S-TECS is directly printed on the upper surface of the reinforced finger body by multi-material 3D printing, and another active layer is made of PDMS and attached to a stretchable electrode. The S-TECS behavior is evaluated for different surface configurations, applied forces and operational frequency using an automated setup. The integrated S-TECS can measure a finger curvature up to 8.2 m^{-1} under an ultra-low working frequency of 0.06 Hz, proving the effectiveness of the proposed S-TECS as a self-powered curvature sensor. This work presents a novel design and fabrication method of S-TECS for its potential applications in multi-material 3D printed soft robotics.

1. Introduction

The aging population poses challenges on labor resources, and the associated labor shortage can be solved by developing robots in areas of medical care, automation manufacturing, and social service [1]. Soft robots, which are made of soft materials and have compliant structures have become attractive solutions to these problems [2,3]. A number of researchers have reported exciting results in the area of soft robotics [4,5], indicating their ability to provide a safe interaction between human, objects, and the environment [6,7]. As a result, soft robots has the potential to bridge the gap between machines and human [3], making it possible to further enrich robot-human and robot-environment applications.

It worth noting that the manufacturing techniques employed to create soft robots are closely linked to their actuator performance and sensory mechanism; the development of new manufacturing technologies can bring a revolution in the field of soft robotics [8]. With the rapid advances in multi-material 3D printing, it is possible to directly print soft robots with an air-tight complex structure and hard components [9,10]. For example, a soft jumping robot was directly printed by multi-material 3D printer to achieve a graded function [11]. In this study, a novel fabrication method to form a soft robot using multi-material 3D printing has been investigated to simplify the prototyping process and enhance the function of the soft body. In our previous research, a fully multi-material 3D printed soft robotic gripper with variable stiffness was developed to ensure robust grasping during high speed movement [12]. Multiple material hardness's were chosen for the soft finger to achieve a variable stiffness within one printing tray. Multi-material 3D printing has significant advantages in fabricating soft robots, such as multiple material selection, it is a one-step printing process and has a short prototyping time [13]. However, lacking of suitable sensors remains a challenge to develop controllable 3D printed

* Corresponding author. State Key Laboratory of Precision Measuring Technology and Instruments, School of Precision Instrument and Optoelectronics Engineering, Tianjin University, Tianjin, 300072, China.
E-mail address: mengying_xie@tju.edu.cn (M. Xie).

https://doi.org/10.1016/j.nanoen.2020.104772
Received 8 January 2020; Received in revised form 29 March 2020; Accepted 30 March 2020
Available online 17 April 2020
2211-2855/© 2020 Elsevier Ltd. All rights reserved.

soft robotics which can fulfill their full potential in practical applications [6]. The ideal sensor for these soft robots needs to have following features: capable of working under a large strain, minimum effect on the actuator response, and easy to be integrated into soft actuator structure.

Soft sensors based on piezoelectric [14–16], conductive [17,18], magnetic [19,20] and organic optical materials [21,22] are the most common options to be integrated into soft robotics. Few challenges remain unsolved when these soft sensors are embedded in the soft robots printed by multi-material 3D printing. First, a complex sensor fabrication process leads to a long prototyping time and limits the potential of mass production. Second, poor performance of the whole system can result from an unstable cable connection and complicated system assembly. Last but not least, difficulties in system integration of a flexible, light and small unit may arise due to the incompatible moduli [23] between the soft body and attached sensors. In response to these limitations, triboelectric sensors have become a practical solution due to its simple working mechanism and self-powered operation [24]. Triboelectric charging is a contact electrification when a material becomes electrically charged after it is separated from a different material, leading to an electric potential difference to drive free electron flowing in the external circuit [25]. Studies have shown the great potential of self-powered triboelectric sensors in applications of human-machine interface [26,27], motion monitoring [28,29], environmental energy harvesting [30–32] and automotive systems [33], as they are excellent candidates to convert mechanical signals into electric signals and realize self-power or self-monitoring. In particular, self-powered triboelectric sensors have reported their potential properties in soft robotics, such as high stretchability [34–36] and good pressure sensitivity [29,37]. Lai et al. have developed a triboelectric pressure-sensing skin, which was able to detect the working states of soft robotic gripper, robotic crawler and robotic finger [37]. In addition, the integrated sensors allow soft robotics actively perceiving and sensing their deformation or response in-real time. A recent study presented a self-powered triboelectric touch sensor based on TangoBlack, a multi-material 3D printed material, and PDMS [38]. It was the first attempt to directly use multi-material 3D printed material as an active triboelectric functional layer. While this sensor has proven the effectiveness of the design, the complex double-electrode structure and carbon-based composite can potentially cause problems in system integration and cable connection. To date, to the best of the authors' knowledge, there is no triboelectric sensor that are directly integrated into soft robotics based on multi-material 3D printing techniques.

In this paper, a novel design and fabrication method are presented to develop a soft robotic finger with triboelectric curvature sensor based on multi-material 3D printing and stretchable electrode. The output voltage of multi-material 3D printed sensors in response to different surface configurations, applied force and operational frequency has been explored. The S-TECS was then successfully integrated into the soft robotic finger, and the integration of the S-TECS does not interfere the flexibility, adaptability or compactability of the whole system. A finger bending motion leads to a contact between two functional layers of the S-TECS, activating the contact electrification and then generating electricity. This proposed S-TECS is able to detect a finger curvature up to 8.2 m^{-1} under a working frequency of 0.06 Hz. The ability to direct print the S-TECS functional triboelectric layer on the body of soft robotic finger has largely reduced the integration complexity of triboelectric sensors into soft robotic system. The outcome of this work has proven that multi-material 3D printing can be used to fabricate not only the soft actuator but also its functional sensor, paving the way towards a simple and fast manufacture process for controllable soft robotics.

2. Materials and methods

2.1. System overview

Fig. 1(a) shows the schematics of the reinforced soft finger with a single-electrode triboelectric curvature sensor (RSF-S-TECS), and the enlarged view of the S-TECS structure can be seen in Fig. 1(b). The bottom active layer of the S-TECS is directly printed on the top surface of the finger body, while the upper active layer is fixed on a 3 mm height spacer at both ends of the finger. The upper layer of the S-TECS is made from a PDMS stretchable electrode, formed by a film casting technique. PDMS was chosen as the other active layer due to its high stretchability, high strength and high electron affinity [39]. Fig. 1(c) shows the image of the developed RSF-S-TECS.

2.2. Design and fabrication

Geometric details of the soft finger are shown in Fig. 2(a). The finger body has nine inflation chambers connected with the main airway. Each inflation chamber has a rectangle shape to provide a flat surface on top to print S-TECS patterns. The hard-reinforced structure has a width of 2 mm. The reinforced structure can increase the maximum pressure durability of the soft finger and reduce its radial expansion. There are two spacers at both ends to support the top layer of S-TECS and maintain an initial distance of 3 mm between two layers of the S-TECS. The bottom strain limiting layer has a thickness of 8 mm. The finger can only bend in one direction according to its chamber configuration. When the finger bends, the top layer of the S-TECS starts to approach to the bottom layer until it makes full contact. While the finger recovers, two layers of the S-TECS start to separate until fully separate.

Fabrication process of the RSF-S-TECS is shown in Fig. 2(b)–(d). The reinforced soft finger with patterns of S-TECS was directly printed using a multi-material 3D printer (Objet350, Stratasys Ltd., USA) as two parts: the reinforced soft main body and the connector. Materials selection and printing setup for each part are shown in Fig. 2(b). Patterns of the S-TECS were directly printed out on the top surface of the finger body to simplify the total fabrication process and to shorten the prototyping time. In this work, AgilusBlack (rubber like, shore A30, elongation at break 250%, tensile strength: 2.75 MPa) was chosen as the functional triboelectric layer and the soft body. The connector, reinforcement structure and spacers were printed by the hardest material that the printer can print, named VeroWhite (high dimensional stability, e-Modulus 2000–3000 MPa). FLX9060 (rubber like, shore A60) was chosen as the material to print a double O-ring sealing mechanism to ensure system airtightness. A glossy finishing was chosen to ensure the smoothness of printed S-TECS pattern. PDMS was chosen as the upper triboelectric layer, and liquid PDMS was directly film casted on a stretchable electrode (COCOMI Ltd., Japan) (Fig. 2(c)). The curing process was carried out at room temperature for 24 h. The fabrication of RSF-S-TECS integrated soft finger was completed when 3D printed parts were connected through a screw mechanism and the top layer of S-TECS was attached to the spacer by silicone adhesive. Fig. 2(e) shows the side view of the assembled RSF-S-TECS.

3. Results and discussion

3.1. Characterization and measurement of S-TECS

A microstructured surface is an excellent candidate of creating the pressure-sensitive triboelectric layer, and the word of "micro" indicates that the size of these features is small compared to the total surface area [37]. To explore the pressure sensitivity of the multi-material 3D printed materials, eight configurations (shown in Fig. 3) were investigated: flat surface of soft material (**S**), flat surface of hard and soft material interval (**S/H**), cuboids of soft material (**C**) (d_1 = 1 mm, h_1 = 0.2, 0.4, 0.6 mm) and pyramids of soft material (**P**) (d_2 = 1 mm, h_2 = 0.2, 0.4, 0.6 mm). Fig. 3(e)–(h) show the tested sensors and Fig. 3(i)–(l) show images of the 3D printed S-TECS microstructured surface, where the black material is AgilusBlack and the white material is Vero White. A smooth finish can be seen from Figure(e)–(f) for sensors with flat surfaces, and fine line patterns were observed from an enlarged view as shown in Fig. 3(i)–(j),

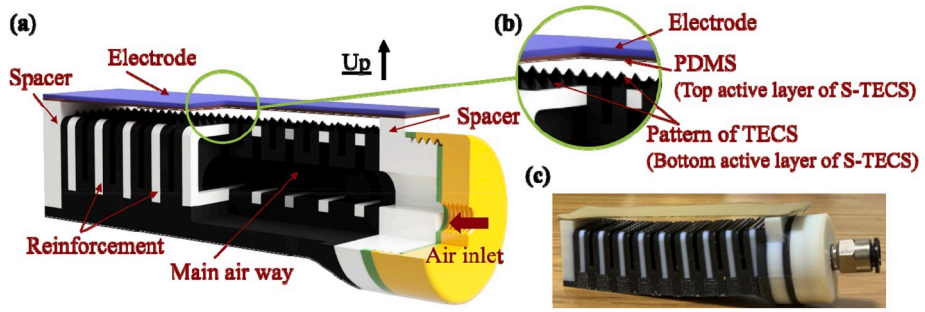

Fig. 1. Multi-material 3D printed reinforced soft finger with triboelectric curvature sensor (RSF-S-TECS). (a) Schematics of the soft finger with a triboelectric curvature sensor located on the top of the soft body. Each color represents a material, where blue is stretchable electrode, red is PDMS, black is AgilusBlack, white and yellow are VeroWhite, green is FLX9060. (b) Enlarged view of the triboelectric curvature sensor. (c) Image of the RSF-S-TECS.

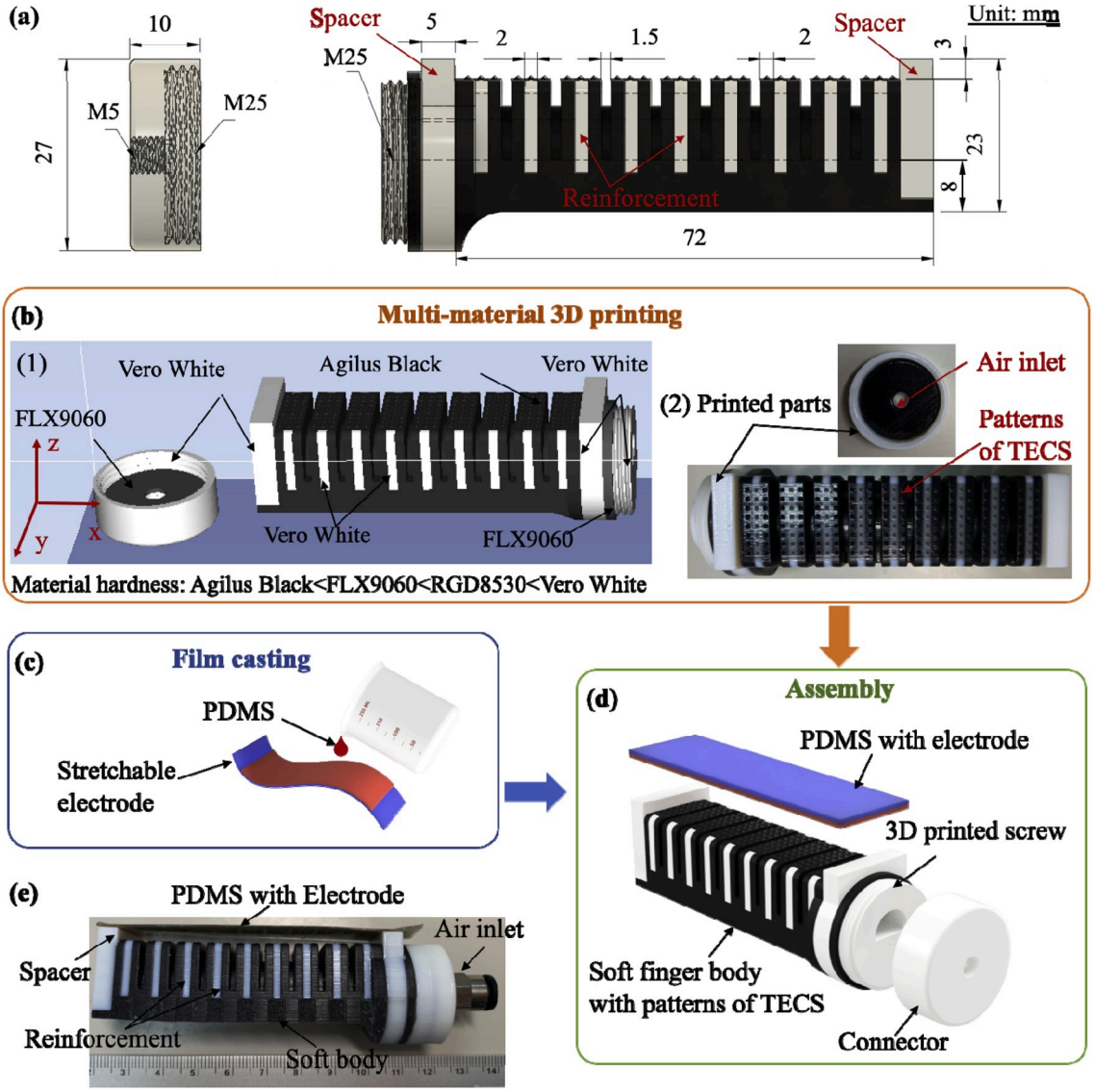

Fig. 2. Design and fabrication process of the reinforced soft finger with triboelectric curvature sensor (RSF-S-TECS) by multi-material 3D printing. (a) Dimension of the reinforced soft robotic finger. (b) Multi-material 3D printing to fabricate the soft finger body with patterns of TECS: (1) Printing environment and material selection for two parts. (2) Printed parts after supporting material removed. (c) Film casting liquid PDMS on stretchable electrode. (d) Assembly process of the RSF-S-TECS: connecting multi-material 3D printed parts through screw mechanist and attaching PDMS with electrode by silicone adhesive. (e) Assembled RSF-S-TECS.

which is similar to the patterns reported by Haque et al. [38]. Sensor configurations of cuboids and pyramids were directly printed out by the 3D printer and it significantly simplified the fabrication process, as shown in Fig. 3(g)–(h). The microstructured surface can be easily fabricated without any additional post-processing. Fig. 3(k)–(l) illustrate that the printed features are regular and consistent, indicating the

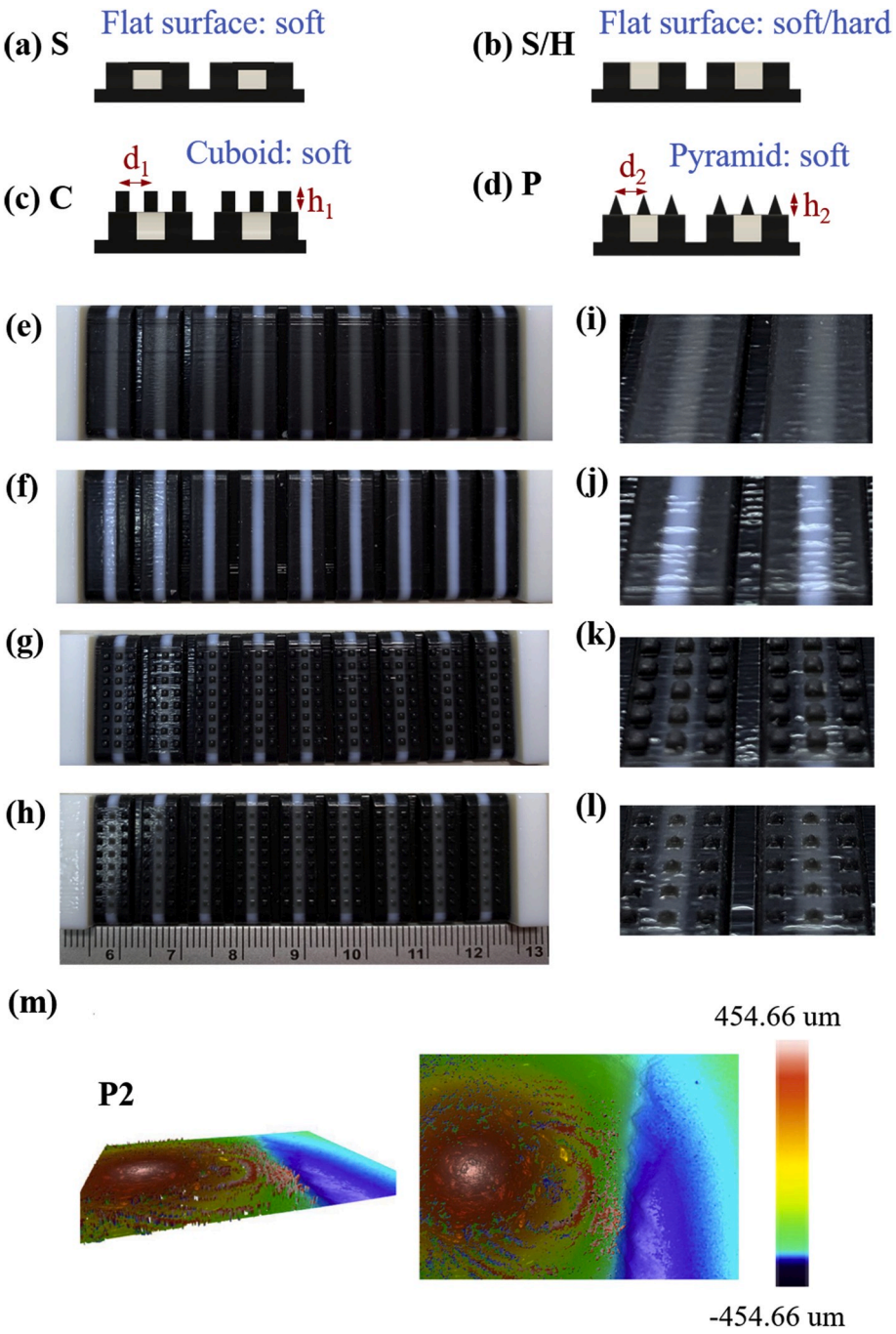

Fig. 3. Surface profile of 3D printed S-TECS. (a)–(d) CAD design of 3D printed triboelectric layer. (a) S: flat surface with soft material. (b) S/H: flat surface with soft and hard material interval. (c) C: soft cuboids. (d) P: soft pyramids. (e)–(h) Images of the multi-material 3D printed sensors. (i)–(l) Images of the multi-material 3D printed microstructured surface. (m) Interference spectrum of the printed pyramids pattern P_2.

effectiveness of the proposed fabrication method.

A custom-made measurement system as shown in Fig. 4(a) was used to supply an external force with different frequencies to the S-TECS. Similar to the previous studies [38], a force gauge was fixed on a linear motor (KZG06030-CA, SURUGA SEIKI CO., Ltd., Japan) to generate cyclic forces up to 45 N and the cycling frequency was controlled by the motor controller. A contacting force was generated when the force gauge was moving downwards, and a triboelectric voltage was generated when the two layers make contact and separate. The open-circuit voltage (V_{OC}) was measured using Keithley 6514 electrometer with high input impedance (>200 TΩ). Fig. 4(b)–(d) shows the V_{OC} responding to series of different forces from 5 N to 45 N for eight surface configurations, i.e. i) flat surface with only soft material (**S**), ii) flat surface with soft hard material interval (**S/H**), iii) cuboids of soft material (**C**) and iv) pyramids of soft material (**P**). In this work, sensor **S** was regarding as the control reference. The instantaneous output voltage linearly increases with increasing contact force for all eight configurations. Among the eight sensors, the configuration with a pyramids pattern with a height of 0.2 mm exhibited the highest peak-to-peak instantaneous voltage (29.9–62.3 V), while the sensor with flat surface made of soft and hard material interval generated the lowest voltage (4.0–13.1 V). This is a result of the varied friction area of the different surface configurations. In Haque's work [38], a multi-material 3D printed touch sensor with flat active layers was investigated. Although

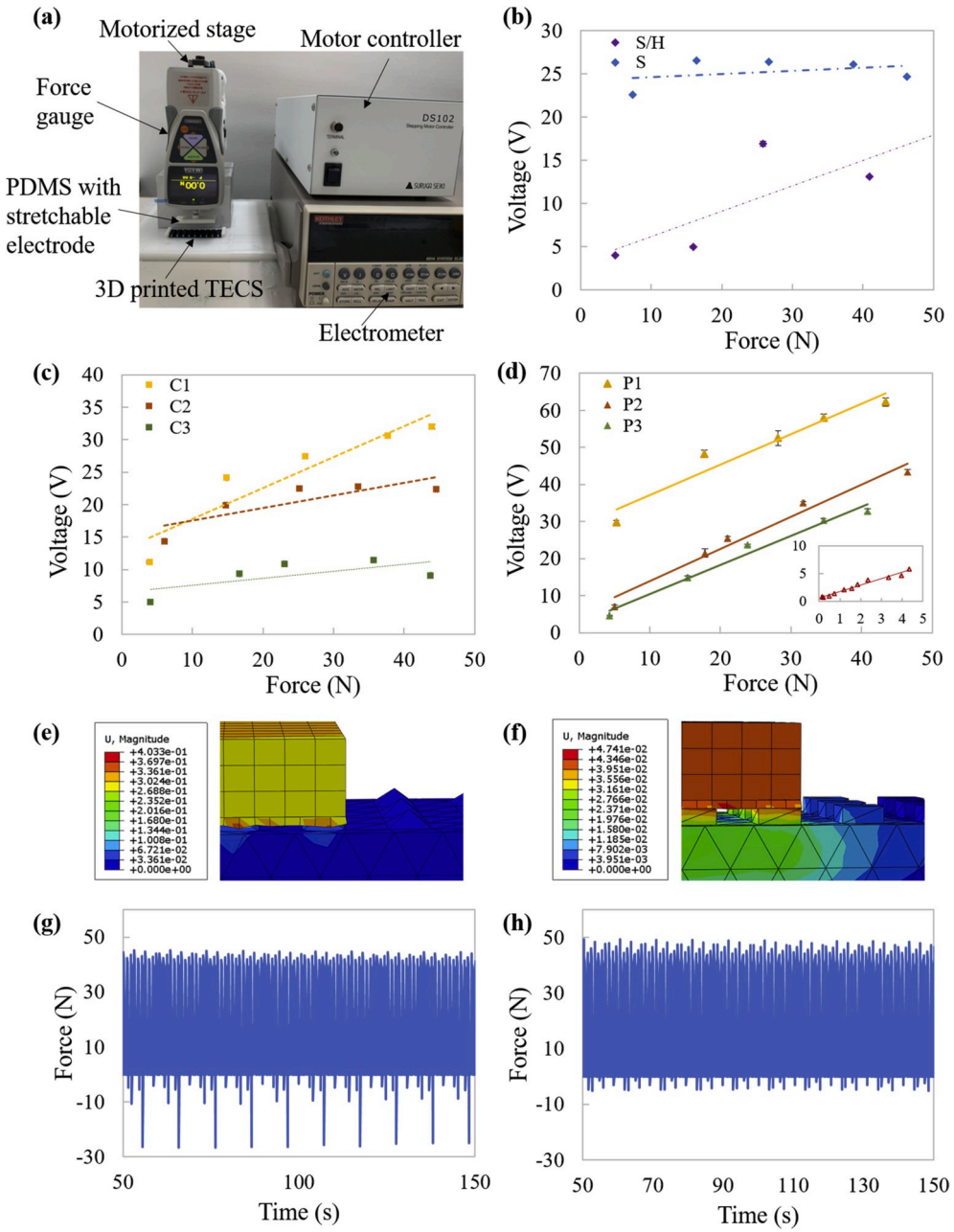

Fig. 4. Experiments on triboelectric output of 3D printed sensors with different surface profile. (a) Experimental setup. (b)–(d) Open-circuit voltage of the 3D printed sensor with different surface profiles. (e)–(f) FEA simulation of sensor deformation for 0.4 mm pyramids and cuboids under the same applied force of 20 N. (g)–(h) Applied force for 0.2 mm and 0.4 mm pyramids.

there was no pattern printed deliberately, due to the nature of multi-material 3D printing method and printing directions, featured line patterns on the soft flat surface and the small features on the paired PDMS layer by casting were found in their touch sensor. Their work nevertheless indicated that these small features can improve the triboelectric efficiency. In Fig. 3(e) and (i), similar line patterns on the sensor **S** can also be observed. However, a strong adhesive phenomenon has been found when a flat soft layer makes contact to PDMS. It is important to ensure the S-TECS does not affect the soft finger's deformation when it is integrated into the system, and the strong adhesive effect between two active layers can interfere the finger deformation and lead to a system response delay. To reduce the adhesion phenomenon, a hard material was introduced onto the soft surface as shown in Fig. 3(f) and (j). Although sensor **S** has a larger generated triboelectric voltage compared to sensor **S/H** (shown in Fig. 4(b)), adding the hard material on the surface can significantly reduce adhesive effect between two layers due to the decreased friction area when the hard material is present.

Then sensors with cuboids and pyramids microstructures were investigated in terms of their ability of increasing sensor's pressure-sensitivity and avoiding the adhesive effect. Fig. 4(c) and (d) show the triboelectric voltage output of cuboids configurations (height of cuboids, $C_1 = 0.2$ mm, $C_2 = 0.4$ mm, $C_3 = 0.6$ mm), and pyramid configurations (height of pyramids, $P_1 = 0.2$ mm, $P_2 = 0.4$ mm, $P_3 = 0.6$ mm), respectively. It can be seen that sensors with a pyramidal microstructure generally generates a larger V_{OC} compared to those with a cuboid microstructure when the height is the same. Here for cuboids microstructures, the stress distribution caused by applied force is constant throughout the height due to the uniform cross-sectional area [40]. Cuboids with a height of 0.2 mm are the most sensitive sensor among three cuboids, while sensitivity of other two cuboids are similar. Studies

have discussed that pyramids are easily deformed under an applied force to create a larger friction area, and have larger air voids to increase effective dielectric constant and triboelectric charges are easily separated with sophisticated structures; these factors lead to a larger triboelectric voltage [41,42]. Finite element modeling (FEM) simulation was carried out in order to study the deformation of different surface pattern (cuboid and pyramid) subjected to normal squeezing. Due to the symmetry, only 1/9 part of the bottom active layer was taken into consideration in FEM simulation. The AgliusBlack as bottom active layer was hyperelastic with material parameters $C_{10} = 0.153$ MPa and $C_{01} = 0.038$ MPa according to Mooney-Rivlin strain-energy function model. A hard slab with a PDMS layer on the top suffers vertical squeezing upon the bottom active layer and just contacts the cuboid or pyramid embossment. Gravity was not considered, thus there was no initial pressure on the bottom active layer. For both surface patterns, a uniform pressure of 20kPa along the vertical direction was applied to the hard slab with PDMS and the deformations is presented in Fig. 4(e)–(f) through a nodal displacement. Since the pyramids are easy to deform, the contact area increases with the deformed pyramids from a partial contact to a full contact (Fig. 4(e)). However, the cuboids have a uniform cross-sectional area which make them less easy to deform and they keep the contact area constant (Fig. 4(f)). As a result, the deformation of the bottom active layer with pyramid pattern is more significant than that with cuboid pattern under the same squeezing pressure. Therefore, sensors with cuboids patterns generate a lower V_{OC} than those with pyramids patterns under the same applied force. In addition, on comparing Fig. 4 (c)–(d), a larger gradient can be found in linear fit of V_{OC} from pyramids than cuboids. Cuboids have uniform cross-sectional area, while pyramids have non-uniform cross-sectional area and the applied pressure is concentrated at the vertex of the pyramid with a small contact area, resulting a large deformation at the tip. The largest gradient of linear fit among cuboid is 0.47 for cuboid with a height of 0.2 mm, while that of pyramids is 0.87 for pyramids with a height of 0.4 mm. As a result, the pyramidal microstructures exhibit a higher sensitivity. In Fig. 4(c)–(d), with the same microstructures, a lower height leads to a higher generated voltage, since microstructures with a small height are easier to deform, leading to a larger friction area [40].

Although sensors with pyramids patterns have a good sensitivity, a noticeable adhesive effect was found for the pyramids with height of 0.2 mm. As pointed out in the previous section, it is important that the developed sensor does not interfere the deformation of the soft finger. A strong adhesive effect can restrict the finger's bending motion and lead to delay in system response. Fig. 4(g) shows the applied force to the 0.2 mm pyramids. A significant negative response can be observed, indicating the adhesive phenomenon between two active layers. By increasing the height of pyramids from 0.2 mm to 0.4 mm, the adhesive affect has been largely reduced, as shown in Fig. 4(h). Pyramids with higher height have a larger sidewall angle and a smaller contact area [43], leading to a subtle adhesive phenomenon.

When these factors are considered, a sensor with pyramidal microstructure of 0.4 mm (P_2) in height was chosen in our study to be further integrated into the complete system. An interference spectrum of printed pyramids can be seen in Fig. 3(m), the measured height of the pyramid P_2 pattern is 426 μm. Fig. 5(a) shows real-time output voltage of sensor P_2 under applied force ranging from 5 N to 45 N, indicating a higher applied force leads to a larger output voltage. Fig. 5(b) shows the open circuit voltage of sensor P_2 across the load resistance value from 10^6 to 10^{12} Ω. To date, the collection of mechanical energy under 1 Hz remains challenging, there are only limited work on harvesting ultralow frequency mechanical energy such as by delicately regulating the applying way in different mechanical waveforms [44]. It is worth noting that operation frequency under 1 Hz has a limited effect on the output voltage of the proposed S-TECS, as shown in Fig. 5(c). The peak-to-peak output voltage of 0.64 Hz was 22% smaller than that of 1.1 Hz.

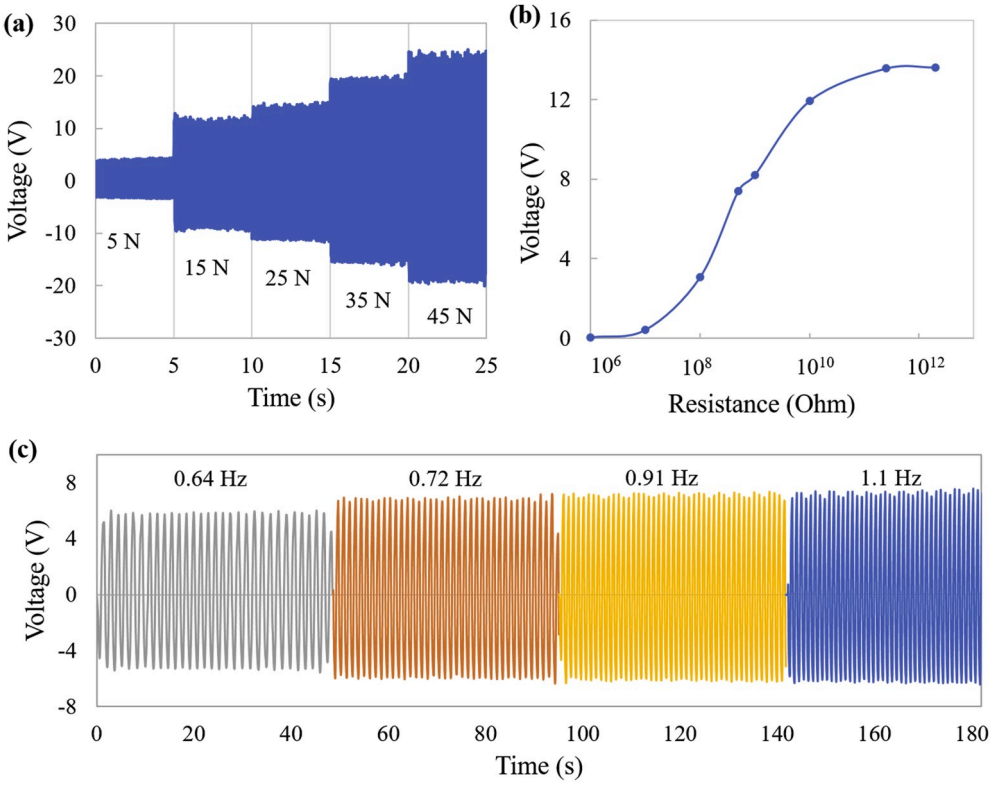

Fig. 5. Experiments on triboelectric output of 3D printed sensor with the surface configuration of 0.4 mm pyramids. (a) Output voltage under applied force from 5 N to 45 N, each force was tested for 35 times. (b) Output voltage with external loads from 0 to 1 TΩ. (c) Output voltage under different operational frequency.

3.2. Influence of the finger bending curvature on the output performance of the S-TECS

When a soft-finger-based gripper is used to grasp an object, the applied inflation pressure can cause a finger deformation to generate a large contact area between the finger and the object. The grasping ability of the gripper is determined by the grasping force generated by actuator deformation and the friction force [45]. The finger curvature which can lead to a large contact area and a compliant motion is important to ensure success and a safe grasp. Herein the developed RSF-S-TECS is able to detect its finger curvature in real-time. A typical working cycle of the RSF-S-TECS is shown in Fig. 6(a). The finger can freely deform in one direction when an inflation pressure is applied through the air inlet. Two layers of the S-TECS are fully separated in the initial condition. When the finger starts to bend, the PDMS with stretchable electrode is stretched and starts to approach the active layer that is directly printed on the finger body. While the bending curvature increases, the friction area between two layers of the S-TECS increases and contact force also increases. The soft finger can bend up to a curvature of 8.2 m^{-1} under an air pressure of 90 kPa. The soft finger recovers to its initial state when the inflation pressure is released. During the recovery process, two layers of the S-TECS start to separate. From snapshot images of the soft finger during a working cycle, it can be observed that the proposed RSF-S-TECS can reversibly switch between the contact and separation states by applying or releasing the inflation pressure. With the reinforced structure, the soft finger can significantly reduce its radial expansion and increase its working pressure compare to our previous work.

Fig. 6(b) shows the schematic of the working principle of the proposed RSF-S-TECS (90° clockwise rotation of Fig. 6(a)). S-TECS has two active layers: an upper layer made of PDMS and bottom layer printed with AgulisBlack. AgulisBlack has a positive charge affinity while PDMS exhibits the highest negative electron affinity [39], making the pair an excellent candidate for electrification and electrostatic induction. When the finger is bent, the PDMS comes in contact with the AgulisBlack patterns which are on the top of soft finger body, and it starts to create a positive potential and electrons flow from the patterned layer to the PDMS to balance the potential difference, leaving positive charges on the AgulisBlack layer and negative charges on PDMS. Once fully contacted, the charges are retained in equilibrium and no electron flow is generated, as shown in Figs. 6(b-1). When the finger returns to its initial state (Figs. 6(b-2)), positive charges are induced on the stretchable electrodes, which resulting in an electron flow from electrode to the ground. When the soft finger recovers to initial state and the PDMS is no longer in contact with the finger body (Figs. 6(b-3)), an electrostatic equilibrium is achieved, and electrons stop flowing. After a cycle once the PDMS comes to contract the soft finger again, a reverse electron flow from the ground to the stretchable electrodes can be found, leading to a voltage of opposite polarity (Figs. 6(b-4)). The same phenomena was also presented in the literature [41,46]. Investigations were carried out to study the relationship between finger's curvature and the output triboelectric voltage. Different finger bending curvature can cause varied friction area and contact force between the S-TECS, leading to an output voltage difference. As we tested in the previous section, the cycling frequency has a limited effect on the proposed S-TECS, further experiments were carried out to quantitatively investigate the RSF-S-TECS output voltage in response to the finger bending curvature only. Experimental setup is shown in Fig. 7(a). The air inlet was connected to an air pump through a positive pressure regulator (ITV2050-212BS). Three colored markers were placed on the soft finger to indicate its curvature (Fig. 6(a)). The finger's movement was captured by a camera during characterization, and data of each marker's position was forward to the computer and the finger's curvature was then calculated. Inflation pressures were applied to cause a finger bending deformation, while the finger curvature was calculated and the real time open-circuit voltage of the S-TECS was monitored. After each test, the inflation pressure was released, and the finger returned to its initial position.

Fig. 7(b) shows the V_{OC} of the S-TECS with applied inflation pressures from 40 kPa to 90 kPa, the corresponding finger curvatures (K) are indicated in the figure. When the pneumatic finger is actuated by an applied pressure, a significant deformation occurs only when the applied pressure reaches the threshold value which is determined by the nature of underlaying material and designed structure. In this study, the threshold value of the finger was 30 kPa. The finger experiences limited deformation when the inflation pressure was below 30 kPa, and two layers of the S-TECS remained separated until the inflation pressure achieves 40 kPa. The output voltage of the S-TECS is determined by two factors: the friction area between two active layers and the contact pressure generated by finger bending. Generally, the larger the bending curvature, the higher the instantaneous output voltage. However, the main factor, the friction area or the contact pressure, is different depending on its condition. As shown in Fig. 7(c), when the finger curvature is small (A-B), the PDMS firstly contacts the pyramid

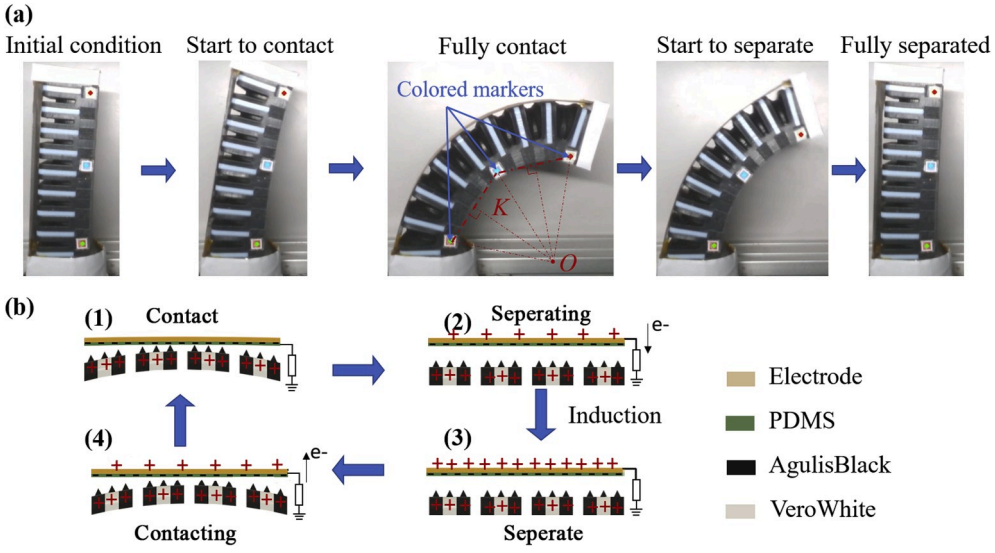

Fig. 6. (a) Snapshots of an RSF-S-TECS in a working cycle. (b) Schematic of the expected charge distribution based on the finger bending position to the top triboelectric layer.

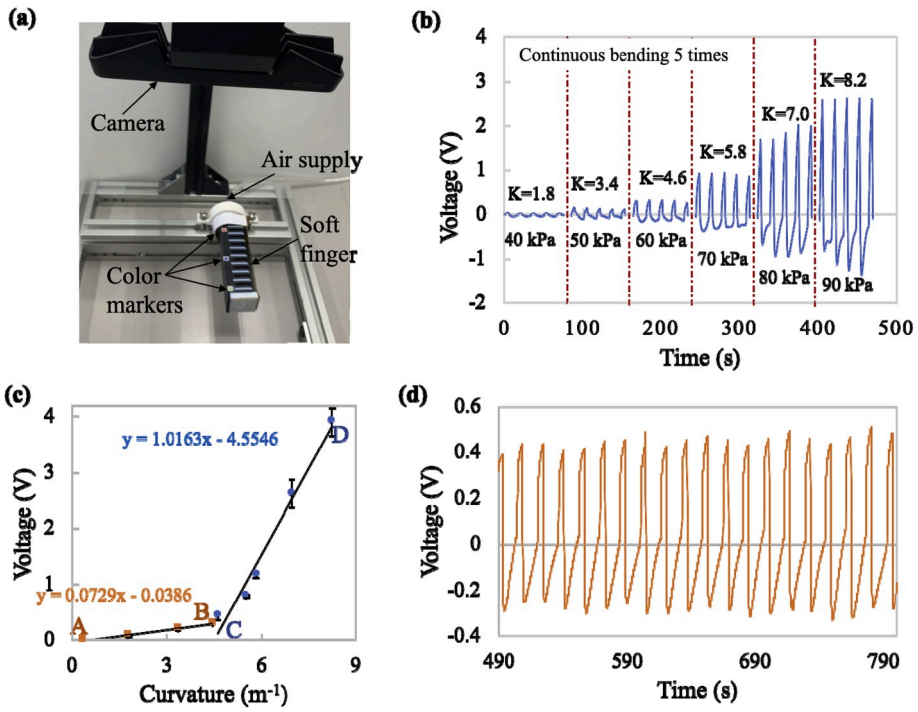

Fig. 7. Characterization on influence of finger bending angle on the output of the S-TECS. (a) Experimental setup for the finger curvature effect on S-TECS output. (b) Output open-circuit voltage in response to varied finger curvature. (c) Linear fitting of the finger curvature to output voltage. (d) Continuous output voltage when finger curvature is 5.5 m^{-1}.

structures and then starts contacting the finger surface. When the finger bends further, the contact surface become larger and the force subjected to the finger surface becomes higher. The main determined factor is the friction area between two active layers, and a small V_{OC} is generated from fully separation to fully contact. In the phase of C-D in Fig. 7(c) where the finger has a large bending curvature the friction area between two layers is unchanged, but a large contact pressure is generated by the finger bending motion, thereby leading to a high V_{OC}. A continuous repeatable output voltage of the RSF-S-TECS when the finger curvature was 5.5 m^{-1} can be seen in Fig. 7(d), proving the repeatability of the proposed S-TECS.

4. Conclusion

This paper presents the directly integration of triboelectric sensors into multi-material 3D printed soft robotics. A soft robotic finger with a self-powered S-TECS based on a multi-material 3D printing has been design, fabricated and demonstrated. The reinforced soft finger and a triboelectric functional layer of the S-TECS were directly printed out by a multi-material 3D printer. PDMS was chosen to be paired with a 3D printed material, AgilusBlack, to construct the S-TECS. A stretchable electrode was used to ensure the developed S-TECS has limited effect on the bending motion of the soft finger. Experiments results have proven that the RSF-S-TECS has ability to sense its finger bending curvature with the developed self-powered triboelectric bending sensor. The multi-material 3D printing technique has provided a novel method to directly print out the soft robotics and its functional sensor within a simple, fast and highly customizable process, paving the way to develop sensor-rich soft robotics for real-world applications. Future work will be carried out on developing closed-loop control of the soft finger curvature by using the developed S-TECS.

Declaration of competing interest

The authors declare that they have no known competing financial interests or personal relationships that could have appeared to influence the work reported in this paper.

CRediT authorship contribution statement

Mingzhu Zhu: Conceptualization, Methodology, Data curation, Investigation, Validation, Writing - original draft. **Mengying Xie:** Conceptualization, Methodology, Software, Investigation, Writing - review & editing. **Xuanming Lu:** Formal analysis. **Shima Okada:** Writing - review & editing. **Sadao Kawamura:** Writing - review & editing, Supervision.

Acknowledgements

This work was supported by the Ritsumeikan Global Innovation Research Organization project, “Robotics Innovation Based on Advanced Materials”, and the MEXT Private University Research Branding project, “Development of a New Sustainable Model for Aged Japanese Society with Ritsumeikan Livelihood Support Sciences”. The work presented in this paper was also partially supported by MEXT Kakenhi 19K14950, JSPS, Japan. The authors would like to thank Dr. Wanfu Shen for the help of Interference Spectrum. The authors would like to thank Prof. Chris Bowen for the help with editing and proof-reading the manuscript.

References

[1] G. Yang, J. Bellingham, P.E. Dupont, P. Fischer, L. Floridi, R. Full, N. Jacobstein, V. Kumar, M. Mcnutt, R. Merrifield, The grand challenges of science robotics, Sci. Robot. 3 (2018), https://doi.org/10.1126/scirobotics.aar7650. UNSP eaar7650.
[2] D. Rus, M.T. Tolley, Design, fabrication and control of soft robots, Nature 521 (2015) 467–475, https://doi.org/10.1038/nature14543.
[3] G.M. Whitesides, Soft robotics, Angew. Chem. Int. Ed. 57 (2018) 4258–4273, https://doi.org/10.1002/anie.201800907.
[4] B. Gorissen, D. Reynaerts, S. Konishi, K. Yoshida, J.W. Kim, M. De Volder, Elastic inflatable Actuators for soft robotic applications, Adv. Mater. 29 (2017) 1–14, https://doi.org/10.1002/adma.201604977.
[5] J. Shintake, V. Cacucciolo, D. Floreano, H. Shea, Soft robotic grippers, Adv. Mater. 1707035 (2018), https://doi.org/10.1002/adma.201707035.

[6] C. Laschi, B. Mazzolai, M. Cianchetti, Soft robotics: technologies and systems pushing the boundaries of robot abilities, Sci. Robot. 1 (2016), https://doi.org/10.1126/scirobotics.aah3690. UNSP eaah3690.
[7] D. Trivedi, C.D. Rahn, W.M. Kier, I.D. Walker, Soft robotics: biological inspiration, state of the art, and future research, Appl. Bionics Biomechanics 5 (2008) 99–117, https://doi.org/10.1080/11762320802557865.
[8] B. Gorissen, D. Reynaerts, S. Konishi, K. Yoshida, J.W. Kim, M. De Volder, Elastic inflatable Actuators for soft robotic applications, Adv. Mater. 29 (2017) 1–14, https://doi.org/10.1002/adma.201604977.
[9] R.L. Truby, J.A. Lewis, Printing soft matter in three dimensions, Nature 540 (2016) 371–378, https://doi.org/10.1038/nature21003.
[10] T.J. Wallin, J. Pikul, R.F. Shepherd, 3D printing of soft robotic systems, Nat. Rev. Mater. 3 (2018) 1–17, https://doi.org/10.1038/s41578-018-0002-2.
[11] N.W. Bartlett, M.T. Tolley, J.T.B. Overvelde, J.C. Weaver, B. Mosadegh, K. Bertoldi, G.M. Whitesides, R.J. Wood, A 3D-printed, functionally graded soft robot powered by combustion, Science 349 (2015) 161–165, https://doi.org/10.1126/science.aab0129 (80-.).
[12] M. Zhu, Y. Mori, T. Wakayama, A. Wada, S. Kawamura, A fully multi-material three-dimensional printed soft gripper with variable stiffness for robust grasping, Soft Robot. (2019) 1–13, https://doi.org/10.1089/soro.2018.0112, 00.
[13] N. Meisel, C. Williams, An investigation of key design for additive manufacturing constraints in multimaterial three-dimensional printing, J. Mech. Des. 137 (2015) 111406, https://doi.org/10.1115/1.4030991.
[14] M. Xie, Y. Zhang, M.J. Krasny, C. Bowen, H. Khanbareh, N. Gathercole, Flexible and active self-powered pressure, shear sensors based on freeze casting ceramic-polymer composites, Energy Environ. Sci. 11 (2018) 2919–2927, https://doi.org/10.1039/c8ee01551a.
[15] T.Q. Trung, N.-E. Lee, Flexible and stretchable physical sensor integrated platforms for wearable human-activity monitoring and personal healthcare, Adv. Mater. 28 (2016) 4338–4372, https://doi.org/10.1002/adma.201504244.
[16] H. Khanbareh, K. de Boom, B. Schelen, R.B.N. Scharff, C.C.L. Wang, S. van der Zwaag, P. Groen, Large area and flexible micro-porous piezoelectric materials for soft robotic skin, Sens. Actuators, A Phys. 263 (2017) 554–562, https://doi.org/10.1016/j.sna.2017.07.001.
[17] Y.L. Park, B.R. Chen, R.J. Wood, Design and fabrication of soft artificial skin using embedded microchannels and liquid conductors, IEEE Sensor. J. 12 (2012) 2711–2718, https://doi.org/10.1109/JSEN.2012.2200790.
[18] C.B. Cooper, K. Arutselvan, Y. Liu, D. Armstrong, Y. Lin, M.R. Khan, J. Genzer, M. D. Dickey, Stretchable capacitive sensors of torsion, strain, and touch using double helix liquid metal fibers, Adv. Funct. Mater. 27 (2017), https://doi.org/10.1002/adfm.201605630.
[19] E. Asadi, H. Askari, M. Behrad Khamesee, A. Khajepour, High frequency nano electromagnetic self-powered sensor: concept, modelling and analysis, Meas. J. Int. Meas. Confed. 107 (2017) 31–40, https://doi.org/10.1016/j.measurement.2017.04.019.
[20] H. Ren, J. Sun, Electromagnetic Actuation and Sensing in Medical Robotics, Springer, 2018, https://doi.org/10.1007/978-981-10-6035-9.
[21] A. Grillet, D. Kinet, J. Witt, M. Schukar, K. Krebber, F. Pirotte, A. Depre, Optical fiber sensors embedded into medical textiles for healthcare monitoring, IEEE Sensor. J. 8 (2008) 1215–1222, https://doi.org/10.1109/JSEN.2008.926518.
[22] J. Peirs, J. Clijnen, D. Reynaerts, H. Van Brussel, P. Herijgers, B. Corteville, S. Boone, A micro optical force sensor for force feedback during minimally invasive robotic surgery, Sens. Actuators A Phys. 115 (2004) 447–455, https://doi.org/10.1016/j.sna.2004.04.057.
[23] J.B. Chossat, Y.L. Park, R.J. Wood, V. Duchaine, A soft strain sensor based on ionic and metal liquids, IEEE Sensor. J. 13 (2013) 3405–3414, https://doi.org/10.1109/JSEN.2013.2263797.
[24] Q. Zheng, B. Shi, Z. Li, Z.L. Wang, Recent progress on piezoelectric and triboelectric energy harvesters in biomedical systems, Adv. Sci. 4 (2017), https://doi.org/10.1002/advs.201700029.
[25] S. Wang, L. Lin, Z. Lin, Triboelectric nanogenerators as self-powered active sensors, Nano Energy 11 (2015) 436–462, https://doi.org/10.1016/j.nanoen.2014.10.034.
[26] W. Ding, A.C. Wang, C. Wu, H. Guo, Z.L. Wang, Human–machine interfacing enabled by triboelectric nanogenerators and tribotronics, Adv. Mater. Technol. 4 (2019) 1800487, https://doi.org/10.1002/admt.201800487.
[27] Y. Jie, H. Zhu, X. Cao, Y. Zhang, N. Wang, L. Zhang, Z.L. Wang, One-piece triboelectric nanosensor for self-triggered alarm system and latent fingerprint detection, ACS Nano 10 (2016) 10366–10372, https://doi.org/10.1021/acsnano.6b06100.
[28] H. Askari, Z. Saadatnia, E. Asadi, A. Khajepour, M.B. Khamesee, J. Zu, A flexible hybridized electromagnetic-triboelectric multi-purpose self-powered sensor, Nano Energy 45 (2018) 319–329, https://doi.org/10.1016/j.nanoen.2018.01.011.
[29] T. Chen, Q. Shi, M. Zhu, T. He, L. Sun, L. Yang, C. Lee, Triboelectric self-powered wearable flexible patch as 3D motion control interface for robotic manipulator, ACS Nano 12 (2018) 11561–11571, https://doi.org/10.1021/acsnano.8b06747.
[30] X. Cao, Y. Jie, N. Wang, Z.L. Wang, Triboelectric nanogenerators driven self-powered electrochemical processes for energy and environmental science, Adv. Energy Mater. 6 (2016), https://doi.org/10.1002/aenm.201600665.
[31] Y. Jie, X. Jia, J. Zou, Y. Chen, N. Wang, Z.L. Wang, X. Cao, Natural leaf made triboelectric nanogenerator for harvesting environmental mechanical energy, Adv. Energy Mater. 8 (2018) 1–7, https://doi.org/10.1002/aenm.201703133.
[32] Y. Jie, Q. Jiang, Y. Zhang, N. Wang, X. Cao, A structural bionic design: from electric organs to systematic triboelectric generators, Nano Energy 27 (2016) 554–560, https://doi.org/10.1016/j.nanoen.2016.07.028.
[33] H. Askari, E. Hashemi, A. Khajepour, M.B. Khamesee, Z.L. Wang, Towards self-powered sensing using nanogenerators for automotive systems, Nano Energy 53 (2018) 1003–1019, https://doi.org/10.1016/j.nanoen.2018.09.032.
[34] H. Chen, L. Bai, T. Li, C. Zhao, J. Zhang, N. Zhang, G. Song, Nano Energy Wearable and robust triboelectric nanogenerator based on crumpled gold fi lms, Nano Energy 46 (2018) 73–80, https://doi.org/10.1016/j.nanoen.2018.01.032.
[35] K. Tao, H. Yi, Y. Yang, H. Chang, J. Wu, L. Tang, Z. Yang, N. Wang, L. Hu, Y. Fu, J. Miao, W. Yuan, Origami-inspired electret-based triboelectric generator for biomechanical and ocean wave energy harvesting, Nano Energy 67 (2020) 104197, https://doi.org/10.1016/j.nanoen.2019.104197.
[36] A. Ahmed, S.L. Zhang, I. Hassan, Z. Saadatnia, Y. Zi, J. Zu, Z.L. Wang, A washable, stretchable, and self-powered human-machine interfacing Triboelectric nanogenerator for wireless communications and soft robotics pressure sensor arrays, Extrem. Mech. Lett. 13 (2017) 25–35, https://doi.org/10.1016/j.eml.2017.01.006.
[37] Y.C. Lai, J. Deng, R. Liu, Y.C. Hsiao, S.L. Zhang, W. Peng, H.M. Wu, X. Wang, Z. L. Wang, Actively perceiving and responsive soft robots enabled by self-powered, highly extensible, and highly sensitive triboelectric proximity- and pressure-sensing skins, Adv. Mater. 30 (2018) 1–12, https://doi.org/10.1002/adma.201801114.
[38] R.I. Haque, O. Chandran, S. Lani, D. Briand, Self-powered triboelectric touch sensor made of 3D printed materials, Nano Energy 52 (2018) 54–62, https://doi.org/10.1016/j.nanoen.2018.07.038.
[39] B.W. Lee, D.E. Orr, The TriboElectric Series, AlphaLab, Inc. (n.d.). https://www.alphalabinc.com/triboelectric-series/(accessed August 28, 2019).
[40] B.C.K. Tee, A. Chortos, R.R. Dunn, G. Schwartz, E. Eason, Z. Bao, Tunable flexible pressure sensors using microstructured elastomer geometries for intuitive electronics, Adv. Funct. Mater. 24 (2014) 5427–5434, https://doi.org/10.1002/adfm.201400712.
[41] F. Fan, L. Lin, G. Zhu, W. Wu, R. Zhang, Z.L. Wang, Transparent triboelectric nanogenerators and self-powered pressure sensors based on micropatterned plastic films, Nano Lett. 12 (2012) 3109–3114, https://doi.org/10.1021/nl300988z.
[42] S.C.B. Mannsfeld, B.C.-K. Tee, R.M. Stoltenberg, C.V.H.-H. Chen, S. Barman, B.V. O. Muir, A.N. Sokolov, C. Reese, Z. Bao, Highly sensitive flexible pressure sensors with microstructured rubber dielectric layers, Nat. Mater. 9 (2010) 859–864, https://doi.org/10.1038/nmat2834.
[43] B.C. Tee, A. Chortos, R.R. Dunn, G. Schwartz, E. Eason, Z. Bao, Tunable Flexible Pressure Sensors Using Microstructured Elastomer Geometries for Intuitive Electronics, 2014, pp. 5427–5434, https://doi.org/10.1002/adfm.201400712.
[44] C. Liu, N. Zhang, J. Li, L. Dong, T. Wang, Z. Wang, Harvesting ultralow frequency (< 1 Hz) mechanical energy using triboelectric nanogenerator, Nano Energy 65 (2019) 104011, https://doi.org/10.1016/j.nanoen.2019.104011.
[45] Y. Wei, Y. Chen, T. Ren, Q. Chen, C. Yan, Y. Yang, Y. Li, A novel, variable stiffness robotic gripper based on integrated soft actuating and particle jamming, Soft Robot. 3 (2016) 134–143, https://doi.org/10.1089/soro.2016.0027.
[46] Y. Yang, H. Zhang, Z.-H. Lin, Y.S. Zhou, Q. Jing, Y. Su, J. Yang, J. Chen, C. Hu, Z. L. Wang, Human skin based triboelectric nanogenerators for harvesting biomechanical energy and as self-powered active tactile sensor system, ACS Nano 7 (2013) 9213–9222, https://doi.org/10.1021/nn403838y.

Mingzhu Zhu received the B.E. degree and the M.E. degree in mechanical engineering from the Nanjing University of Science and Technology, Nanjing, China, in 2009 and 2011; and the Ph. D. degree in Mechatronics Engineering from the University of Auckland, New Zealand in 2016. She was a senior researcher in Ritsumeikan Global Innovation Research Organization (R-GIRO) (2016-2019). She is currently a faculty member in Zhejiang University of Technology. Her research area includes soft robotics and soft sensors.

Mengying Xie received the B.Sc.degree in applied physics from Tianjin University, China in 2010 and a Ph.D. degree in mechatronics engineering from the University of Auckland, New Zealand in 2015. She worked in NEMESIS project in University of Bath as a postdoc (2016-2018) and as a senior researcher in Ritsumeikan University (2018-2019). She is currently an associate professor in Tianjin University. Her research area includes energy harvesting and its applications, including water splitting, self-powered sensors, and other wearable electronics.

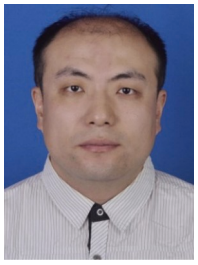

Xuanming Lu received the B. E. degree in mechanical engineering and automation in 2010 from Nanjing University of Science and Technology, China where he got the Ph. D. degree in mechanical engineering in 2019. He is currently a lecturer in the Research Department of Intelligent Manufacturing Equipment, Nanjing Institute of Technology. He was with the Faculty of Engineering, The University of Auckland, New Zealand on leave from Nanjing University of Science and Technology during 2013–2017 with a Doctoral Scholarship from the China Scholarship Council. His main research field includes soft robots, biomimetic robots and pneumatic technology.

Shima Okada received the B.E. degree and the M.E. degree in science and engineering from Ritsumeikan University, Japan, in 2000 and 2002; and the Ph.D. degree in Medical Sciences from Osaka University in 2008. She is currently an associate professor in College of Science and Engineering in Ritsumeikan University. Her research area includes medical systems, applied health science, perception information processing/intelligent robotics, sensitivity informatics/soft computing.

Sadao Kawamura received a B.S. degree in Biophysical Engineering (1981), a M.S. degree in Mechanical Engineering (1983) and a PhD in Mechanical Engineering (1986) from Osaka University. He is currently a professor in the Department of Robotics in Ritsumeikan University. His research area includes soft robotics, underwater robots, sensor integrated control, high energy efficient robots, extremely lightweight robots.